OPEN ACCESS
Journal of Innovative Optical Health Sciences
Vol. 17, No. 2 (2024) 2450001 (10 pages)

DOI: 10.1142/S1793545824500019

World Scientific
www.worldscientific.com

Geometric regulation of collective cell tangential ordering migration

Hao Dong*, Yuming Zhou*, Xuehe Ma*, Junfang Liu*, Fulin Xing*, Jianyu Yang*, Qiushuo Sun*, Qingsong Hu*, Fen Hu*,¶, Leiting Pan*,†,‡,§,‖ and Jingjun Xu*,‡

*The Key Laboratory of Weak-Light Nonlinear Photonics of Education Ministry
School of Physics and TEDA Institute of Applied Physics
Nankai University
Tianjin 300071, P. R. China

†State Key Laboratory of Medicinal Chemical Biology
Frontiers Science Center for Cell Responses
College of Life Sciences
Nankai University
Tianjin 300071, P. R. China

‡Shenzhen Research Institute of Nankai University
Shenzhen, Guangdong
518083, P. R. China

§Collaborative Innovation Center of Extreme Optics
Shanxi University
Taiyuan, Shanxi 030006, P. R. China
¶hufen@nankai.edu.cn
‖plt@nankai.edu.cn

Received 2 January 2024
Accepted 21 January 2024
Published 5 March 2024

Collective cell migration is a coordinated movement of multi-cell systems essential for various processes throughout life. The collective motions often occur under spatial restrictions, hallmarked by the collective rotation of epithelial cells confined in circular substrates. Here, we aim to explore how geometric shapes of confinement regulate this collective cell movement. We develop quantitative methods for cell velocity orientation analysis, and find that boundary cells exhibit stronger tangential ordering migration than inner cells in circular pattern. Furthermore, decreased tangential ordering movement capability of collective cells in triangular and square patterns are observed, due to the disturbance of cell motion at unsmooth corners of these patterns. On the other hand, the collective cell rotation is slightly affected by a convex defect of the circular pattern, while almost hindered with a concave defect, also resulting from different

¶,‖Corresponding authors. Leiting Pan is the lead contact.

smoothness features of their boundaries. Numerical simulations employing cell Potts model well reproduce and extend experimental observations. Together, our results highlight the importance of boundary smoothness in the regulation of collective cell tangential ordering migration.

Keywords: Collective cell migration; spatial restrictions; tangential ordering; geometric regulation; cell Potts model.

1. Introduction

Cell migration is a fundamental biological process in embryonic development, wound healing, immune defense, and cancer metastasis.[1–3] Compared with single-cell migration, collective cells exhibit more intricate coordinated dynamic behaviors, analogous to other active matter systems that also contain large amounts of active units such as fish shoals,[4] bird flocks[5] as well as artificial active particles.[6] The emergence and evolution of collective cell migration is closely related to extracellular microenvironment, such as substrate geometry[7–9] and stiffness.[10,11] Interestingly, utilizing cell micropatterning technology to provide external spatial restrictions enables a diversity of ordering collective cell migration phenomena, involving coordinated rotation in circular constraints,[12] wavelike oscillation in quasi-one-dimensional channel,[13] as well as sheet migration on narrow parallel stripes.[14]

Among these ordered behaviors, the collective tangential ordering rotation of epithelial cells has attracted extensive attention, owing to its crucial roles in morphogenesis and tissue formation. For instance, such collective rotation is commonly existed in follicular epithelial cells of *Drosophila* ovum,[15] and mammary epithelial acinus,[16] as a key player for the establishment of follicle or acinar structure and the formation of ducts. It has been well established that the occurrence and persistence of this rotation motion relies on sustained memory of cell polarity and strong cell-to-cell adhesion characteristics of epithelial cells.[17] *In vitro*, the collective rotation behavior has been studied in constraint shapes of circles,[12,17,18] and circle-derived patterns such as rings[19,20] or spheres.[21] Besides, in circular confinement, the collective rotation only emerges within a limited size range, while cells form local vortices with overall disorder rather than global ordering movement in large sizes of patterns.[17,22] However, the actual *in vivo* microenvironments are more complex and variable, the shapes of the boundary that limits cells cannot be perfect circles. Whether collective cell rotation can take place in other shapes of micropatterns, and how boundary geometry affects the collective cell movement still call for further exploration.

To address these issues, in this study, we investigated the collective migration behaviors of Madin-Darby canine kidney (MDCK) cells restricted in micropatterns including regular polygons and concave-convex defective circles. We developed innovative analysis methods for quantitative comparison of cell migration orientation between varying pattern shapes. Additionally, simulations based on cell Potts model were executed to illuminate the universal laws of geometric regulation.

2. Materials and Methods

2.1. *Cell culture*

MDCK epithelial cells were maintained in Dulbecco's modified Eagle's medium (Gibco, USA) supplemented with 10% (v/v) fetal bovine serum (Biological Industries, USA) and 1% penicillin and 1% streptomycin (Gibco, USA) at 37°C, 5% CO_2. Time-lapse imaging was performed on an inverted optical differential interference contrast microscope (Ti-E, Nikon, Japan) equipped with an incubator (INUB-ZILCSGH-F1, Tokai Hit, Japan) at 37°C with 5% CO_2 under humidified atmosphere. Images were collected every 5 min by an sCMOS (ORCA-flash4.0, Hamamatsu, Japan) controlled with Micro-Manager 1.4 software (NIH, USA).

2.2. *Fabrication of micropatterned substrates*

Micropatterned substrates were prepared as we previously described.[23,24] Briefly, utilizing photolithography technology, we transferred the designed patterns on photomask to the clean glass coverslips. The regions outside the pattern were passivated by 200 μg/ml poly-l-lysine-poly (ethylene glycol)-silane (pLL-PEG) (SuSoS, Switzerland) solution for 1 h. Subsequently, the micropatterned area is functionalized by coating with 20 μg/mL fibronectin

(FN, BD, USA) for 1 h. After that, MDCK cells were seeded onto the substrates at 37°C for 1 h in prior to remove nonadherent cells by washing with the culture medium.

2.3. *Particle image velocimetry and ordering parameter analysis*

The velocity fields of cell populations were quantified by particle image velocimetry (PIV) analysis based on MATLAB (MathWorks), with a $24 \times 24\ \mu m^2$ interrogation window and 75% overlap. To assess the orderliness of cell motion, we defined ordering parameter $D(t) = |\frac{1}{N}\sum \cos\theta(t)|$, where θ is the acute angle between the direction of cell velocity and the tangential direction of pattern, $\theta \in [-\pi/2, \pi/2]$, N is the number of θ counted. $D \in [0, 1]$, a value closer to 1 denotes higher tangential orderliness of the cell movement.

2.4. *Analysis of directional angle distribution*

To quantitatively evaluate the orientation of cell movement, we developed a method of directional angle distribution. The distribution curve of the directional angles θ exhibited a symmetry along zero degree, and can be well fitted with the equation:

$$p = P_1 * \frac{1}{\sqrt{2\pi}\sigma} \exp\left(-\frac{\theta^2}{2\sigma^2}\right) + \frac{P_2}{\pi}, \qquad (1)$$

where P_1 is the proportion of cells whose velocity vectors obeying Gaussian distribution, σ stands for the standard deviation of Gaussian distribution, and P_2 is the proportion of cells whose velocity vectors following uniform distribution. Since $P_1 + P_2 = 1$, there are only two independent parameters of P_1 and σ in this formula. Accordingly, there exists two modes of cell movement, that is, oriented mode obeying Gaussian distribution with standard deviation σ, and random mode following uniform distribution. A greater value of P_1 and a smaller value of σ means more tangentially migrating cells in the cell population, namely, a stronger orientation of collective cell movement.

2.5. *Analysis of isotropy index*

To assess the orientation of cell movement at a specific spatial position, we defined isotropy index γ based on the gained velocity fields. Specifically, taking any orientation as the primary axis and its perpendicular orientation as the secondary axis, we projected the velocity vectors at all time points onto the primary and secondary axis, respectively, and calculated the sum of their absolute values ($\sum |V_b|$ and $\sum |V_a|$), thereby deriving their ratio $\gamma_0 = \frac{\sum |V_b|}{\sum |V_a|}$. By traversing all possible directions, the yielded minimum value γ_0 represents the isotropic index γ at the corresponding position. $\gamma \in [0, 1]$, a value of 1 means an isotropic motion orientation, and the closer it is to 0, the stronger the orientation.

2.6. *Actin dynamics-based cell Potts model*

Cell Potts model is a classical model widely used in the simulation of single cell and collective cell migration owing to its well description of cell shape changes and cell-to-cell interactions.[25–27] The cell behaviors in the model depends on the energy H of the whole system. Whether a change can be accepted is up to the energy difference ΔH of the system after and before this change. The smaller ΔH, the higher the probability $e^{-\Delta H/T}$ that the system will accept the change, where T is the system temperature. Here, the energy of the system is derived from cell surface mechanics and the cellular cytoskeleton. The energy of cell surface mechanics H_{CSM} is expressed as

$$H_{CSM} = \sum_{i,j} J(\sigma_i, \sigma_j)(1 - \delta_{\sigma_i,\sigma_j}) + \sum_{\sigma} \lambda_{Area}(a_\sigma - A_\sigma)^2 + \sum_{\sigma} \lambda_{Perimeter}(p_\sigma - P_\sigma)^2, \qquad (2)$$

where i and j are neighboring grid sites, σ is the cell identity, a_σ is cell area, p_σ is cell perimeter. The three terms of Eq. (2) describe the adhesion energy, volume energy, and perimeter energy of cells, respectively. Importantly, actin activity V_{act} is introduced to the model for consideration of the contribution of cytoskeleton to cell migration.[28] Newly formed grids of one cell will be assigned with maximum actin activity $(V_{act})_{max}$, and the actin activity of all grids will decrease by 1 every Monte Carlo step (MCS) until it reaches zero. When copying grid i to j, the energy difference provided by actin ΔH_{act} is represented as

$$\Delta H_{act} = -\frac{\lambda_{act}}{(V_{act})_{max}}[GM(j) - GM(i)], \qquad (3)$$

where λ_{act} is the maximum contribution of actin to H, and GM(i) represents the geometric mean of the activity values in the neighborhood of i within the same cell. Cells can achieve directed migration through spontaneous polarization of actin. Moreover, to simulate geometric confinement in the experiment, we introduce the adhesion energy $H_{substrate}$ between cells and the substrate. For the FN region, we set $H_{substrate} = 0$ to allow cells to adhere. In contrast, for the PEG region, we set $H_{substrate} = 10,000$, creating a high-energy barrier to prevent cells from migrating outside the pattern. For ease of statistics, the step size is set to 20,000 MCSs for all simulations. The number of simulated cells is 40, close to experimental number. The values of all simulation parameters are shown in Table S1.

2.7. *Statistical analysis*

All data are presented as mean ± standard error of mean (SEM) from at least three independent experiments or simulations. The statistical comparison between the two groups was carried out using Student's t-test (OriginPro 2022, OriginLab). Statistical significance was defined as $^{*}p < 0.05$, $^{**}p < 0.01$, $^{***}p < 0.001$, $^{****}p < 0.0001$, NS, not significant ($p > 0.05$).

3. Results

3.1. *Boundary cells show stronger tangential ordered migration than inner cells in circular pattern*

Firstly, we analyzed the velocity field of MDCK cells confined in 200 μm-diameter circular micropatterns based on PIV (Fig. 1(a) and Movie S1). It clearly manifested a tangential rotation behavior of collective cells, corroborating previous studies.[12,17,18] Results showed that the ordering parameters D (See more details in *Materials and methods* 2.3) were almost stabilized at a high level (>0.5) during a period of ∼15 h, indicating the coherence of cell rotation rather than transient vortex (Fig. 1(a)). Based on a developed analysis method of directional angle distribution (See more details in *Materials and methods* 2.4), we plotted the distribution curves of all the cells in the pattern, the cells of inner circle and outer ring during the same period, respectively, all of which can be well fitted with

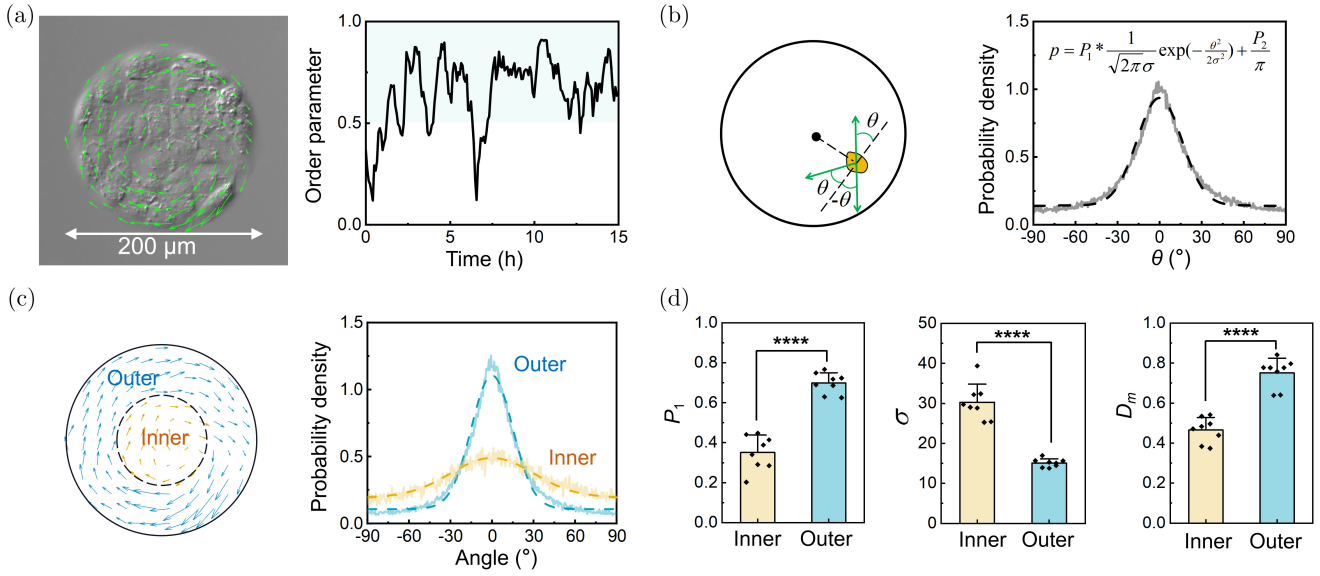

Fig. 1. The collective migration of MDCK cells in circular pattern. (a) PIV analysis showing the velocity field of MDCK cells confined to a 200 μm-diameter circular pattern (left), and the evolution of corresponding order parameter D (right). The shaded area indicates $D > 0.5$. (b) The deviation of the cell velocity direction from the tangential direction described by an acute angle θ (left). Positive θ represents the cell moves outward and negative means inward. The distribution curve of θ (solid line) for all the cells in the pattern, which is fitted (dash line) by Eq. (1) (right). (c) The distribution curves of θ (solid line) and fitting curves (dash line) for inner circle and outer ring, respectively. The radius of the inner circle is half of the whole circle. (d) Comparison of P_1, σ, and D_m between inner circle and outer ring ($n = 7$, mean ± SEM, $^{****}p < 0.0001$, pair t-test).

Eq. (1), obeying a superposition of Gaussian and uniform distribution (Figs. 1(b) and 1(c)). The proportion of cells with tangential oriented migration mode is P_1, with standard deviation σ. The outer ring cells derived a significantly larger P_1, smaller σ, as well as greater mean order parameter $D_m (D_m = \langle D(t) \rangle_t)$ than those of the inner circle cells (Fig. 1(d)), indicating the cell movement near the boundary is with stronger tangential order than that inside the circle.

3.2. *Collective cell tangential ordered migration is inhibited in both square and triangular patterns*

We next explored the velocity field of collective cells constrained in square (Fig. 2(a) and Movie S2) and regular triangular (Fig. 2(b) and Movie S3) micropatterns with 200 μm-side length, comparable to the 200 μm-diameter circular pattern. Sustained collective cell rotation occurred in neither pattern, with smaller ordering parameters (< 0.5) for most of the 15 h-period (Figs. 2(a) and 2(b)). Afterward, the θ distributions (Figs. S1(a) and S1(b)) and D_m were analyzed, with defining the geometric center of the pattern as the center of rotation. Compared with the values of circular pattern, square and triangular patterns had sequentially smaller P_1, larger σ, and lower D_m (Fig. 2(c)), suggesting the tangential ordering cell migration is largely suppressed in both patterns. Besides, the orientation of cell movement in triangular pattern is weaker than that in square pattern.

To elucidate underlying mechanisms, we analyzed the motion characteristics of cells near the boundaries. Kymograph of cell positions obviously showed disturbance of cell orientation at the corners of the boundary (Fig. 2(d)). We further exploited a means of isotropy index analysis to obtain the orientation of cell movement at all spatial locations within the pattern (See more details in *Materials and methods* 2.5) (Fig. 2(e)). The smaller the value of isotropy index γ, the stronger the orientation of cell migration. Through plotting the heatmaps of isotropy index γ for the three patterns, we found that the region with low γ values is dramatically

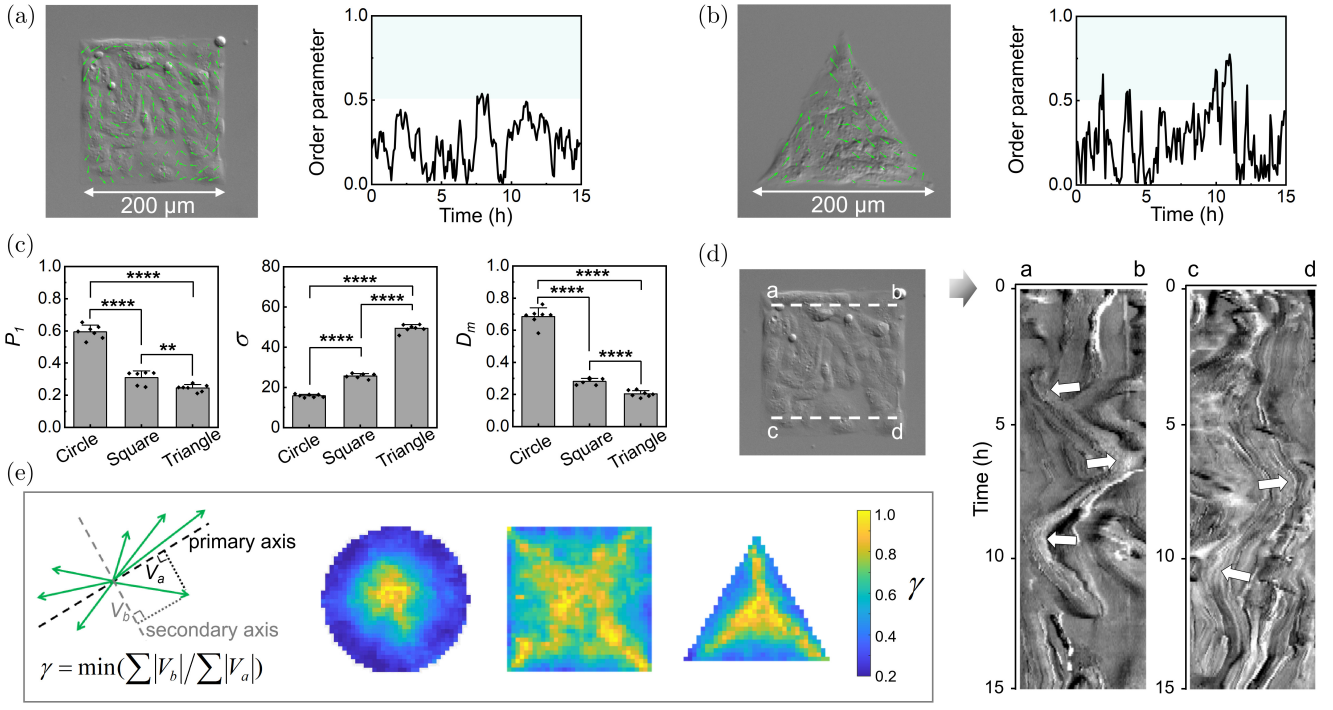

Fig. 2. The collective migration of MDCK cells in square and triangular patterns. (a) and (b) PIV analysis for collective cells confined to a square (a) and a regular triangular (b) pattern with 200 μm-side length (left) and the evolution of corresponding order parameter D (right). (c) Summary of P_1, σ, and D_m in different shapes ($n = 7$, 6, 7 for circular, square, and triangular pattern, respectively, mean $\pm$ SEM, $^{**}p < 0.01$, $^{****}p < 0.0001$, two sample t-test). (d) Spatiotemporal displacement of cells traced along the edge "a−b" and "c−d". The arrows indicate that cell movement transforms to the opposite direction when encountering the corner. (e) Illustration of isotropic index γ (left) and its heatmaps for circular, square, and triangular pattern (right).

interrupted in both patterns in comparison with circular pattern, due to the extremely high γ values at the angular bisector of boundary corners (Fig. 2 (e)). Therefore, the unsmooth boundary shapes with corners may result in interruption of cell directional movement around the boundary, thereby failing to form coherent cell tangential ordered migration.

3.3. *Collective cell rotation is differentially regulated by concave and convex defects of circular pattern*

Subsequently, we studied the collective cell movement in defective circular micropatterns. Results showed that the collective cell rotation was strongly blocked in concave defective circular patterns with 200 μm diameter (Fig. 3(a) and Movie S4). In contrast, continuous cell rotation could still take place in convex defective ones, as shown by high order parameters (>0.5) for a relative long duration (Fig. 3(b) and Movie S5). The analyses of θ distributions (Figs. S1(c) and S1(d)) and order parameters indicated greater P_1 and D_m values of concave patterns than convex ones (Fig. 3(c)), strengthening the distinct regulatory effects on collective cell rotation between concave and convex defects.

Similarly, we analyzed the cell movement near the defects to clarify this discrepancy. The heatmaps of γ showed that the cell orientation markedly decreased at the sharp corners of the concave defect, hence interrupting the low γ region around the boundary and consequently leading to cessation of cell rotation (Fig. 3(d)). On the contrary, the smoother convex defect maintained coherent low values of γ around the entire pattern boundary without evident disturbance, resulting in slighter influence on the collective cell rotation (Fig. 3(d)). These results imply the different smoothness natures of concave and convex restriction boundary account for the varied regulation.

3.4. *Simulations of collective cell tangential ordered migration in varying pattern shapes based on cell Potts model*

By numerical modeling employing a cell Potts model with proper parameters based on the experiments (See more details in *Materials and methods* 2.6), we successfully reproduce the collective cell rotation phenomenon in circular restrictions (Figs. 4(a) and 4(b), Movie S6). From the simulation, the θ distribution obeys superposition of Gaussian and uniform distribution (Fig. 4(c)), consistent with experimental results (Fig. 1(b)).

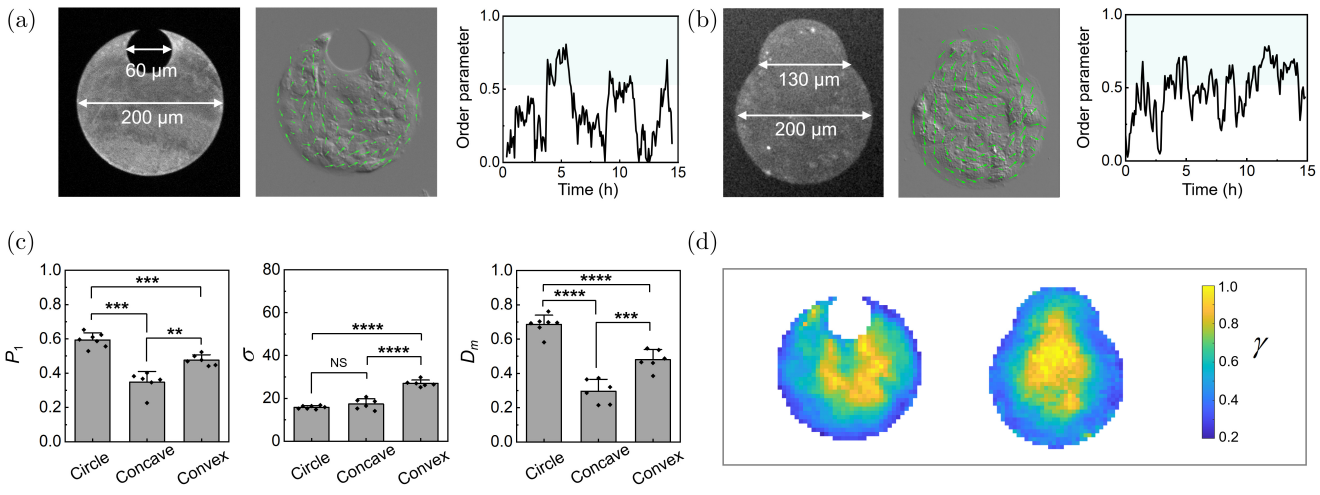

Fig. 3. The collective migration of MDCK cells in defective circular micropatterns. (a) and (b) PIV analysis for collective cells confined to circular micropatterns with a concave defect (a) and a convex defect (b) (left), and the evolution of their order parameter D (right). (c) Summary of P_1, σ, D_m in different shapes ($n = 7, 6, 6$ for normal, concave defective and convex defective circular patterns, respectively, mean ± SEM, NS, no significance, $^{**}p < 0.01$, $^{***}p < 0.001$, $^{****}p < 0.0001$, two sample t-test). (d) Heatmaps of isotropy index γ for concave and convex defective circular patterns.

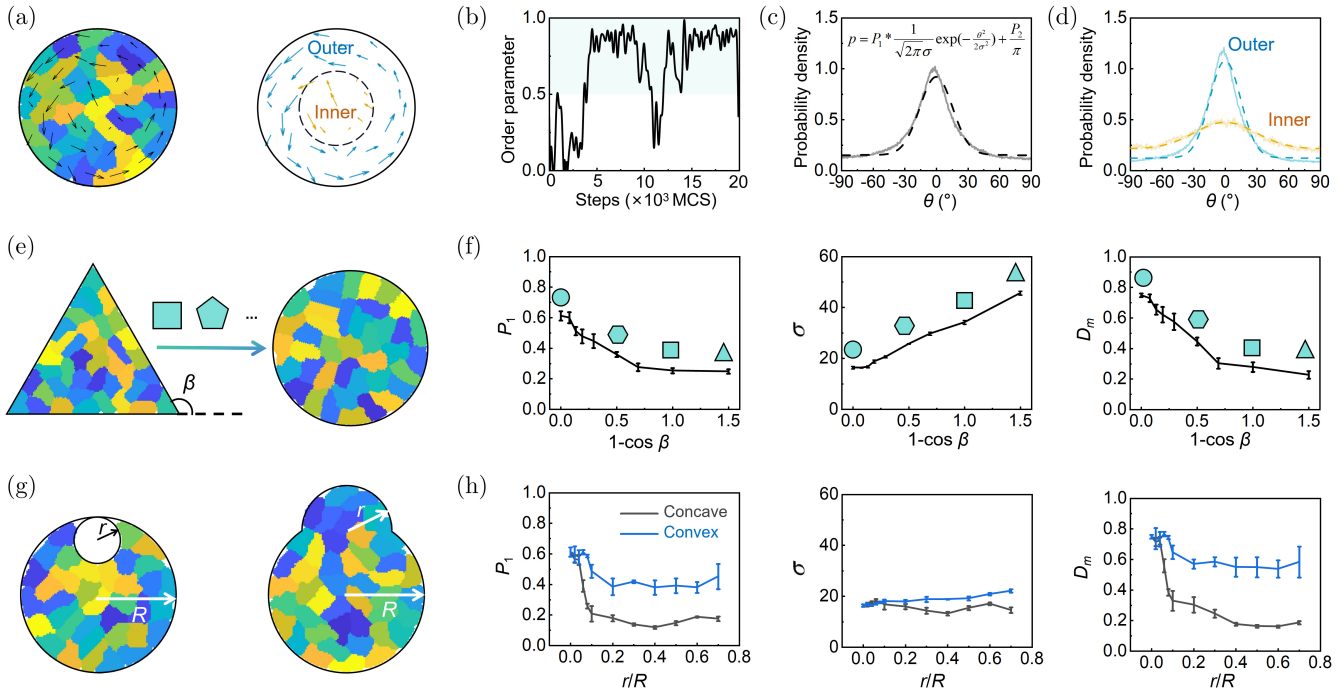

Fig. 4. Numerical simulations of collective cell migration in varying pattern shapes. (a) Simulations of cells confined to a circular pattern. (b) Evolution of corresponding order parameter D in (a). (c) and (d) Distribution curves of θ (solid line) and fitting curves (dash line) for the whole circle (c), inner circle and outer ring (d), respectively. (e) Simulations of cells confined to regular polygon patterns with increased sides number. (f) Summary of P_1, σ, and D_m for varied shapes ($n = 3$ for each group, mean ± SEM). (g) Simulations of cells confined on concave and convex defective patterns. (h) Summary of P_1, σ, and D_m for varied defective radius r (keep R constant).

Importantly, simulations also support a stronger motion orientation of outer ring cells (Fig. 4(d)), validating the reliability of the model.

Furthermore, simulations on the migration behaviors of collective cells in various regular polygons are performed, from regular triangle, square, pentagon, ... eventually approaching circle (Fig. 4(e) and Movie S7). With the increase of polygon sides number, the exterior angles of polygons gradually decrease to 0°, resulting in smoother boundaries. The smoothness is described by $1 - \cos\beta$, a smaller value represents smoother border (Fig. 4(f)). Analyses of the θ distributions (Fig. S2(a)) and order parameters showed that the smoother the boundary, the greater the values of P_1 and D_m, and the smaller the value of σ (Fig. 4(f)). These results elucidate a more general rule that increasing boundary smoothness lead to stronger orientation of cell motion, thus facilitating the collective cell tangential ordering migration.

Meanwhile, simulations for concave-convex defects of circular pattern (Fig. 4(g), Figs. S2(b), S2(c) and Movie S8) reveal that the directional movement of cells is more sensitive to the concave defects with less smooth boundary, namely, only a subtle defect radius can completely block the cell rotation (Fig. 4(h)). By contrast, convex defects have less influence, as shown by moderate decline of P_1 and D_m along with the defect radius (Fig. 4(h)). These simulations further unveil that the concave-convex defect nature per se determines the overall orientation of collective cells, regardless of the defect sizes.

4. Discussion

Nowadays, there has been growing interest in collective cell migration, an essential process in the lives of multicellular organisms.[1–3,29,30] Especially, considerable literature focus on a fascinating coordinated rotation behavior of epithelial cells within spatial limitations.[12,17–21] In this study, to mimic the complicated microenvironment in physiological conditions, we created diversified geometry of confining substrates applying photolithography technology. Thereby, we attempted to figure out the geometric regulatory roles and potential mechanisms on collective cell migration.

Gaining inspiration from PIV analysis of cell velocity field, we first exploited a quantitative method of directional angle distribution (Figs. 1(a) and 1(b)). Through fitting the distribution results with typical equations, we strikingly found it precisely obeys a superimposing of Gaussian and uniform distribution, corresponding to the oriented- and random-migrating cells, respectively (Fig. 1(b)). Traditional order parameter analysis is commonly used to estimate the overall orderliness of cell movement.[17,22] In comparison, our approach not only provides the orientation information of single cells, but also quantitatively describes different migration modes in a cell population. By such means, it revealed stronger orientation of boundary cells than interior cells during the migration (Figs. 1(c) and 1(d)), indicating collective cells in the circular island do not rotate synchronously like a solid disk, instead, boundary cells dominate the global oriented motion. Interestingly, a previous work on migration behaviors of oligocellular systems (two to eight cells) constrained to circular pattern[12] was in accordance with our cognition on the poor orientation of inner cells, and their work suggested this poor orientation may interfere with the stability of cell rotation.

From the results of triangular and square micropatterns, we intriguingly observed that cells reversed their direction and exhibited an oscillatory motion when they encounter unsmooth corners of the boundary (Fig. 2(d)), akin to the wave-like movement of MDCK cells confined to quasi-one-dimensional channels.[13] By developing a method of isotropy index to analyze the orientation of cell movement at each spatial location within the pattern, we clearly visualized the incoherence of cell orientation in both patterns, with abrupt changes at the angular bisector (Fig. 2(e)), which may be the cause of inconsecutive collective cell tangential migration. Moreover, similar disturbance of cell motion was also observed at the sharp corners of the concave defective circular patterns rather than the smoother convex ones (Fig. 3(d)). Thus, the cell tangential migration will be interrupted at the unsmooth corners in a pattern, which may result in a transition from collective ordered rotation to a wave-like oscillation or other types of disordered movement.

Besides, the relative less sensitivity of collective cell rotation to convex defects from both experiments (Fig. 3) and simulations (Fig. 4) implicated that convex circular restriction boundaries are more likely to appear in actual physiological processes such as the rotation of follicular or acinar epithelial cells,[15,16] because of their better "fault tolerance". Instead, concave ones should be completely excluded from actual conditions. However, it should be noted that despite the overall poor orientation, the concave circular pattern has a lower σ (Fig. 3(c)), which may arise from the narrowing of the area below the concave defect, causing the movement direction of local cells more concentrated.

5. Conclusions

Based on novel data analysis methods together with numerical simulations, our work reveals the regulation of collective cell tangential ordering migration by the smoothness nature of the geometric restriction. The smoother the boundary, the higher possibility for the formation of coherent collective cell tangential ordering migration. Disturbance of cell movement occurs at the crossing angles of unsmooth boundaries, leading to pronounced discontinuity of collective cell behavior. These findings provide novel insights into the migration dynamics of collective cells in complex confining spaces, as well as enriching our understanding of momentous biological processes including embryogenesis and morphogenesis. It will also aid the design ideas and manufacturing strategies in tissue engineering.

Acknowledgments

This work was supported by the National Natural Science Foundation of China (Nos. 12174208 and 32227802), National Key Research and Development Program of China (No. 2022YFC3400600), Guangdong Major Project of Basic and Applied Basic Research (No. 2020B0301030009), Fundamental Research Funds for the Central Universities (Nos. 2122021337 and 2122021405), and the 111 Project (No. B23045).

Conflicts of Interest

The authors declare that there are no conflicts of interest relevant to this paper.

Supporting Information

The material is available at https://www.worldscientific.com/doi/suppl/10.1142/S1793545824500019

References

1. R. Mayor, S. Etienne-Manneville, "The front and rear of collective cell migration," *Nat. Rev. Mol. Cell Biol.* **17**(2), 97–109 (2016).
2. X. Trepat, E. Sahai, "Mesoscale physical principles of collective cell organization," *Nat. Phys.* **14**(7), 671–682 (2018).
3. W. Xi, T. B. Saw, D. Delacour, C. T. Lim, B. Ladoux, "Material approaches to active tissue mechanics," *Nat. Rev. Mater.* **4**(1), 23–44 (2019).
4. L. Gómez-Nava, R. T. Lange, P. P. Klamser, J. Lukas, L. Arias-Rodriguez, D. Bierbach, J. Krause, H. Sprekeler, P. Romanczuk, "Fish shoals resemble a stochastic excitable system driven by environmental perturbations," *Nat. Phys.* **19**(5), 663–669 (2023).
5. A. Cavagna, A. Cimarelli, I. Giardina, G. Parisi, R. Santagati, F. Stefanini, M. Viale, "Scale-free correlations in starling flocks," *Proc. Natl. Acad. Sci. USA* **107**(26), 11865–11870 (2010).
6. H. R. Vutukuri, M. Hoore, C. Abaurrea-Velasco, L. van Buren, A. Dutto, T. Auth, D. A. Fedosov, G. Gompper, J. Vermant, "Active particles induce large shape deformations in giant lipid vesicles," *Nature* **586**(7827), 52–56 (2020).
7. S. R. K. Vedula, H. Hirata, M. H. Nai, A. Brugués, Y. Toyama, X. Trepat, C. T. Lim, B. Ladoux, "Epithelial bridges maintain tissue integrity during collective cell migration," *Nat. Mater.* **13**(1), 87–96 (2014).
8. D. Mohammed, G. Charras, E. Vercruysse, M. Versaevel, J. Lantoine, L. Alaimo, C. Bruyère, M. Luciano, K. Glinel, G. Delhaye, O. Théodoly, S. Gabriele, "Substrate area confinement is a key determinant of cell velocity in collective migration," *Nat. Phys.* **15**(8), 858–866 (2019).
9. S. Tlili, M. Durande, C. Gay, B. Ladoux, F. Graner, H. Delanoë-Ayari, "Migrating epithelial monolayer flows like a Maxwell viscoelastic liquid," *Phys. Rev. Lett.* **125**(8), 088102 (2020).
10. M. E. Pallarès, I. Pi-Jaumà, I. C. Fortunato, V. Grazu, M. Gómez-González, P. Roca-Cusachs, J. M. de la Fuente, R. Alert, R. Sunyer, J. Casademunt, X. Trepat, "Stiffness-dependent active wetting enables optimal collective cell durotaxis," *Nat. Phys.* **19**(2), 279–289 (2023).
11. S. Sonam, L. Balasubramaniam, S.-Z. Lin, Y. M. Y. Ivan, I. Pi-Jaumà, C. Jebane, M. Karnat, Y. Toyama, P. Marcq, J. Prost, R.-M. Mège, J.-F. Rupprecht, B. Ladoux, "Mechanical stress driven by rigidity sensing governs epithelial stability," *Nat. Phys.* **19**(1), 132–141 (2023).
12. F. J. Segerer, F. Thüroff, A. Piera Alberola, E. Frey, J. O. Rädler, "Emergence and persistence of collective cell migration on small circular micropatterns," *Phys. Rev. Lett.* **114**(22), 228102 (2015).
13. V. Petrolli, M. Le Goff, M. Tadrous, K. Martens, C. Allier, O. Mandula, L. Hervé, S. Henkes, R. Sknepnek, T. Boudou, G. Cappello, M. Balland, "Confinement-induced transition between wavelike collective cell migration modes," *Phys. Rev. Lett.* **122**(16), 168101 (2019).
14. S. R. K. Vedula, M. C. Leong, T. L. Lai, P. Hersen, A. J. Kabla, C. T. Lim, B. Ladoux, "Emerging modes of collective cell migration induced by geometrical constraints," *Proc. Natl. Acad. Sci. USA* **109**(32), 12974–12979 (2012).
15. H. Wang, S. Lacoche, L. Huang, B. Xue, S. K. Muthuswamy, "Rotational motion during three-dimensional morphogenesis of mammary epithelial acini relates to laminin matrix assembly," *Proc. Natl. Acad. Sci. USA* **110**(1), 163–168 (2013).
16. M. Cetera, G. R. Ramirez-San Juan, P. W. Oakes, L. Lewellyn, M. J. Fairchild, G. Tanentzapf, M. L. Gardel, S. Horne-Badovinac, "Epithelial rotation promotes the global alignment of contractile actin bundles during drosophila egg chamber elongation," *Nat. Commun.* **5**(1), 5511 (2014).
17. K. Doxzen, S. R. K. Vedula, M. C. Leong, H. Hirata, N. S. Gov, A. J. Kabla, B. Ladoux, C. T. Lim, "Guidance of collective cell migration by substrate geometry," *Integr. Biol.* **5**(8), 1026 (2013).
18. M. Deforet, V. Hakim, H. G. Yevick, G. Duclos, P. Silberzan, "Emergence of collective modes and tri-dimensional structures from epithelial confinement," *Nat. Commun.* **5**(1), 3747 (2014).
19. S. Jain, V. M. L. Cachoux, G. H. N. S. Narayana, S. de Beco, J. D'Alessandro, V. Cellerin, T. Chen, M. L. Heuzé, P. Marcq, R.-M. Mège, A. J. Kabla, C. T. Lim, B. Ladoux, "The role of single-cell mechanical behaviour and polarity in driving collective cell migration," *Nat. Phys.* **16**(7), 802–809 (2020).
20. A. Glentis, C. Blanch-Mercader, L. Balasubramaniam, T. B. Saw, J. d'Alessandro, S. Janel, A. Douanier, B. Delaval, F. Lafont, C. T. Lim, D. Delacour, J. Prost, W. Xi, B. Ladoux, "The emergence of spontaneous coordinated epithelial rotation on cylindrical curved surfaces," *Sci. Adv.* **8**(37), eabn5406 (2022).
21. A. S. Chin, K. E. Worley, P. Ray, G. Kaur, J. Fan, L. Q. Wan, "Epithelial cell chirality revealed by three-dimensional spontaneous rotation," *Proc. Natl. Acad. Sci.USA* **115**(48), 12188–12193 (2018).

22. S.-Z. Lin, S. Ye, G.-K. Xu, B. Li, X.-Q. Feng, "Dynamic migration modes of collective cells," *Biophys. J.* **115**(9), 1826–1835 (2018).
23. F. Xing, H. Dong, J. Yang, C. Fan, M. Hou, P. Zhang, F. Hu, J. Zhou, L. Chen, L. Pan, J. Xu, "Mesenchymal migration on adhesive–nonadhesive alternate surfaces in macrophages," *Adv. Sci.* **10** (23), e2301337 (2023).
24. F. Xing, H. Zhang, M. Li, H. Dong, X. Ma, S. Deng, F. Hu, I. Lee, L. Pan, J. Xu, "Regulation of actin cytoskeleton via photolithographic micropatterning," *J. Innov. Opt. Health Sci.* **16**(02), 2244005 (2023).
25. F. Graner and J. A. Glazier, "Simulation of biological cell sorting using a two-dimensional extended Potts model," *Phys. Rev. Lett.* **69**(13), 2013–2016 (1992).
26. F. Thüroff, A. Goychuk, M. Reiter, E. Frey, "Bridging the gap between single-cell migration and collective dynamics," *eLife* **8**, e46842 (2019).
27. R. Alert, X. Trepat, "Physical Models of Collective Cell Migration," *Annu. Rev. Condens. Matter Phys.* **11**(1), 77–101 (2020).
28. I. Niculescu, J. Textor, R. J. de Boer, "Crawling and gliding: A computational model for shape-driven cell migration," *PLOS Comput. Biol.* **11**(10), e1004280 (2015).
29. H. Zhao, T. Ji, T. Sun, H. Liu, Y. Liu, D. Chen, Y. Wang, Y. Tan, J. Zeng, H. Qiu, Y. Gu, "Comparative study on photobiomodulation between 630 nm and 810 nm LED in diabetic wound healing both *in vitro* and *in vivo*," *J. Innov. Opt. Health Sci.* **15**(02), 2250010 (2022).
30. D. Yang, Z. Yuan, Z. Yang, M. Hu, Y. Liang, "High-resolution polarization-sensitive optical coherence tomography and optical coherence tomography angiography for zebrafish skin imaging," *J. Innov. Opt. Health Sci.* **14**(06), 2150022 (2021).